


Tunable coupling between InSb nanowires and superconductors

Ghada Badawy ¹, Marcel A. Verheijen,² and Erik P. A. M. Bakkers^{1,*}

¹*Applied Physics Department, Eindhoven University of Technology, 5600 MB Eindhoven, The Netherlands*

²*Eurofins Material Science Netherlands B.V., High Tech Campus 11, 5656 AE Eindhoven, The Netherlands*



(Received 22 September 2022; accepted 21 December 2022; published 12 January 2023)

The quest for topological states in hybrid nanowire devices has ignited substantial research in perfecting the nanowire-superconductor interface. Recent proposals, however, suggest that these immaculate interfaces can lead to an overly strong superconducting-semiconducting coupling that “metalizes” the nanowire (i.e., dominates its intrinsic properties which are essential for hosting topological particles). One way to reduce this coupling is to add an insulating shell between the nanowire and the superconductor. Here, we explore cadmium telluride (CdTe) shells as a tunnel barrier at the interface between indium antimonide (InSb) nanowires and a superconductor. We demonstrate the growth of epitaxial, defect-free CdTe on InSb and high-quality superconductor deposition at cryogenic temperatures, enabled by the near perfect lattice match of CdTe and InSb and their comparable thermal-expansion coefficients. Using growth and etching, we control the thickness of CdTe shells down to a few monolayers. This level of control indicates the potential of these shells to serve as a knob that modulates the coupling between a nanowire and a superconductor, possibly introducing a new generation of nanowire hybrids suitable for topological Majorana devices.

DOI: [10.1103/PhysRevMaterials.7.016201](https://doi.org/10.1103/PhysRevMaterials.7.016201)

I. INTRODUCTION

Topological quantum circuits are among the candidates for quantum computing due to the promise of fault tolerance [1–3]. Among the platforms to realize these circuits [4–6] are semiconducting-superconducting nanowire hybrids [7,8], which require a semiconducting nanowire with strong spin-orbit interaction and a large Landé g factor contacted by a conventional s -wave superconductor [9–12]. This setup is predicted to transform the nanowire into a topological superconductor with Majorana fermions localized at its ends [13,14], owing to the interplay between the proximity-induced superconductivity, the intrinsic nanowire properties, and the Zeeman splitting (induced by an external magnetic field).

Topological superconductivity in one-dimensional nanostructures demands stringent material requirements, including defect-free nanowires coupled to superconductors via smooth and clean interfaces. Several studies have demonstrated nearly defect-free nanowires coupled to superconducting shells [15–18]. The quality of the smooth and clean—and often epitaxial—superconductor-semiconductor interfaces is corroborated by an induced superconducting gap free of any subgap states—a hard superconducting gap [15,16,19,20].

Nevertheless, proposals argue that the outstanding quality of these interfaces might be unfavorable [21–23]. Specifically, they result in an overly strong coupling, causing the superconductor to outweigh the intrinsic properties of the nanowire, e.g., its spin-orbit coupling and Landé g factor. This strong coupling leads to an induced gap nearly identical to that of the superconductor, casting doubt on whether the properties

of the nanowire are at all relevant and, in turn, critically disputing whether the nanowire can undergo a topological phase transition [21–23].

One way to reduce the coupling between the superconductor and the nanowire is to introduce a thin insulating layer at their interface to serve as a tunnel barrier.

In this work, we explore cadmium telluride (CdTe) as an insulating layer between indium antimonide (InSb) nanowires and superconducting shells of aluminum (Al) and lead (Pb). The CdTe layer is in the form of a concentric shell around the nanowire (schematic in Fig. 1) and serves as a tunnel barrier between the superconductor and the nanowire with the shell thickness determining coupling strength, as shown in Fig. 1. The precise control of the shell thicknesses down to a few monolayers is achieved using both growth and etching of the CdTe. The CdTe shells promote epitaxial growth of superconductor shells and support abrupt, smooth, and clean interfaces. The deposition conditions that enable the realization of these high-quality superconducting shells are examined. The absence of visible defects and disorder in the CdTe shells along with the largely epitaxial superconducting shells with impeccable interfaces ensure a uniform coupling strength along the entire superconductor-semiconductor interface. The atomic-level control of the thickness provides a control knob to fine tune the superconducting-semiconducting coupling, potentially facilitating the realization of topological superconductivity in nanowire hybrids and enabling the unambiguous detection of Majorana quasiparticles.

II. CDTE SHELLS AS TUNNEL BARRIERS

InSb is a promising semiconductor for the research of topological devices owing to its strong spin-orbit coupling

*e.p.a.m.bakkers@tue.nl

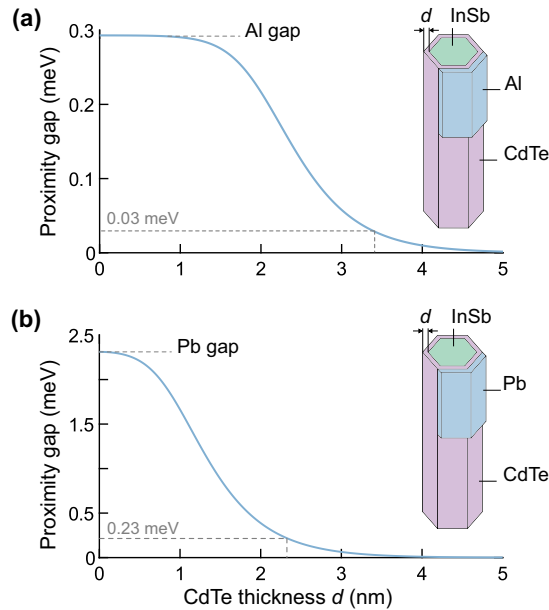


FIG. 1. Adjustable CdTe shell thickness as a tunable tunnel barrier between the superconducting shell and the InSb nanowire. The proximity-induced gap as a function of CdTe shell (tunnel barrier) thickness d , for both (a) Al and (b) Pb. The CdTe thickness d is adjustable, allowing precise tuning of the coupling strength between the nanowire and the superconductor. The coupling strength is quantified by the size of the proximity-induced gap (see Sec. S1 of the Supplemental Material for details of the calculation [24]). For an induced gap, 10% of the bulk superconducting gap, a CdTe thickness of 3.4 nm is required for Al compared to 2.3 nm for Pb, as indicated by the dashed lines. The insets show schematics of the trilayer stack composing the InSb nanowire, the CdTe shell, and a partial superconducting shell, Al and Pb, respectively.

and its large Landé g factor. InSb also exhibits a narrow band gap of 0.17 eV and a large bulk electron mobility, of the order of $77\,000\text{ cm}^2/\text{Vs}$. To induce superconductivity in an InSb nanowire, it is coupled to a conventional superconductor. Adding a CdTe layer in the form of a concentric shell around the nanowire to interface with the superconductor (Fig. 1) allows for the controlled modulation of the superconductor-semiconductor coupling strength. The choice of CdTe is motivated by its large band gap (1.5 eV) relative to InSb [25] and the near lattice match to InSb with a difference in lattice constants of roughly 0.004 \AA [26,27]. In addition, the identical crystal structures, cubic zinc blende, enable the growth of defect-free CdTe shells surrounding the InSb nanowires. These properties allow for the CdTe shells to serve as a tunnel barrier while preserving the pristine quality of the InSb nanowire. Moreover, the nearly identical thermal-expansion coefficients of InSb and CdTe enable the cryogenic deposition of the superconductor without instigating defects or stress to the nanowire. The structural compatibility of CdTe with InSb renders it an ideal material candidate to act as a tunable tunnel barrier at the interface between InSb and a superconductor. In particular, the coupling strength can be modulated as a function of the thickness of the CdTe layer and can be quantified by the magnitude of the induced superconducting gap (Fig. 1). To span the entire range of coupling strengths, covering both

the strong- and the weak-coupling limits, the CdTe thickness is varied from 0.5 to 5 nm. Generally, a reduced coupling strength leads to a smaller proximity-induced gap, compared to the bulk gap of the superconductor.

We estimate the size of the induced gap as a function of CdTe shell thickness in Fig. 1. This estimate is based on the transmission probability of Cooper pairs across a rectangular barrier with thickness d . Moreover, the size of the induced gap depends on the effective mass of electrons in the CdTe and the barrier height, which corresponds to the conduction-band offset at the InSb-CdTe interface [25]. Details on this approximation can be found in Sec. S1 of the Supplemental Material [24] (see, also, Refs. [28,29] therein). Because weaker coupling keeps any disorder in the superconductor away from the semiconductor, we consider a weak-coupling limit for which the induced gap constitutes 10% of the bulk superconducting gap [22]. As shown in Fig. 1, the required CdTe thickness is dependent on the choice of superconductor. The schematics in Fig. 1 show that the superconductor is deposited on the CdTe shell to complete a trilayer stack composing the InSb nanowire, the CdTe tunnel barrier, and the superconductor. The superconductor is deposited on the CdTe shell to partially cover it, rather than surround it. This partial coverage facilitates the electronic tunability of the Fermi level of the nanowire by external gating. As Fig. 1 conveys, the studied superconductors are aluminum (Al) and lead (Pb). The focus in this work is on aluminum, as it is the prototypical superconductor for Majorana experiments [14,16,30,31] as well as other quantum information processing circuits [32]. Further, the rationale behind using Pb along with initial results on its epitaxial deposition are discussed.

III. CDTE SHELLS THICKNESS CONTROL

The CdTe shells surround the InSb nanowire by covering its six $\{110\}$ facets. The InSb nanowires are grown with the vapor-liquid-solid (VLS) method using gold catalyst particles on masked InSb (111)B substrates, as detailed in [33], while the growth details of epitaxial, defect-free CdTe shells are presented in [25]. The thickness control over the epitaxial CdTe shells is achieved either by varying the growth time or, alternatively, by etching the grown shells using atomic hydrogen in a molecular beam epitaxy (MBE) chamber.

With regards to controlling the CdTe thickness by varying the growth time, the CdTe shell thickness follows a linear increase once layer closure is completed, as summarized in Fig. 2. In particular, the early stages of growth are dominated by island growth, followed by linear growth after roughly 30 minutes. As shown in Fig. 2(a), the distinct growth regimes are likely attributed to different nucleation kinetics on InSb compared to CdTe. That is, nucleation of CdTe on InSb proceeds slower compared to the homo-epitaxial nucleation of CdTe on CdTe. The shell growth proceeds via the hetero-epitaxial nucleation of crystalline islands, which extend and merge into a single crystalline shell [Fig. 2(c)]. The continuous, monocrystalline CdTe shell in Fig. 2(c) is roughly 2.5 nm thick and displays the typical cubic atomic stacking of the zinc-blende crystal structure when viewed along the $\langle 110 \rangle$ zone axis in high-resolution scanning TEM without signs of oxidation. For growth times shorter than 30 minutes, the crystalline

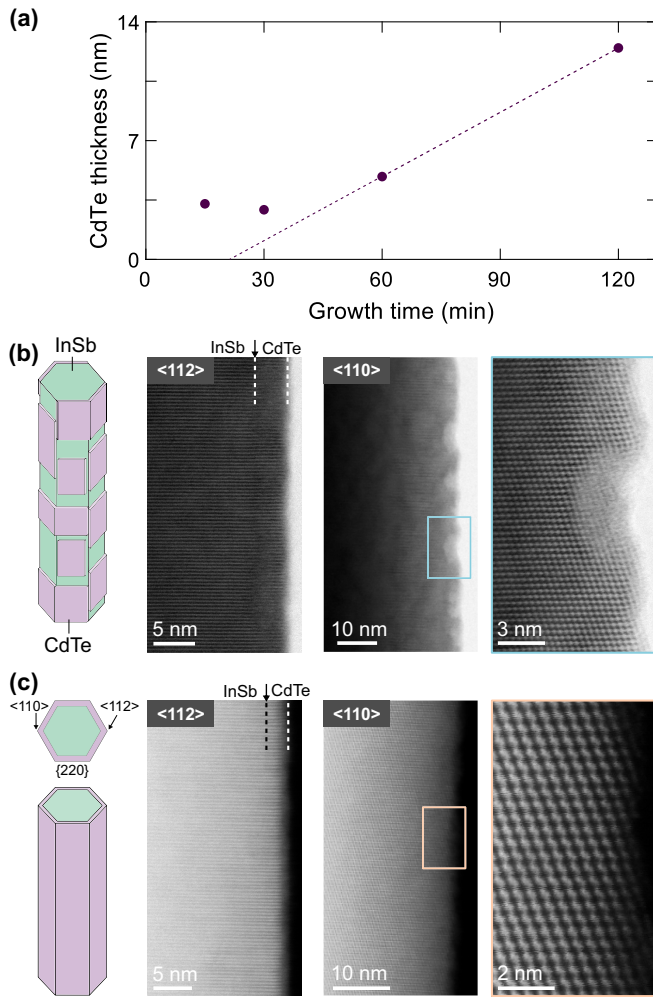


FIG. 2. Growth of CdTe shells. (a) The CdTe thickness as a function of growth time evolves from island growth to linear growth. Error bars fall within the size of the data marker. For growth times less than 30 minutes, the shells are discontinuous and their thickness is overestimated by TEM. (b) A schematic and TEM scans of a discontinuous shell. The discontinuity is not visible along the $\langle 112 \rangle$ zone axis (parallel to a side facet), but is visible along the $\langle 110 \rangle$ zone axis at the corner between two side facets [as schematically depicted in the hexagon in (c)]. The visible cusps in the shells are amorphous as disclosed by the high-resolution TEM image of the framed region. Within these cusps, the InSb is locally oxidized. (c) A continuous CdTe shell grown for 30 minutes. In the high-angle annular dark-field images taken along the $\langle 112 \rangle$ and $\langle 110 \rangle$ zone axes, smooth facets are evident. The CdTe shell is nearly indistinguishable from the InSb core because they have similar atomic numbers. The InSb-CdTe interface is, thus, specified by an arrow according to the measured CdTe thickness. The thickness is determined using ADF imaging, used in Figs. 3(c) and 3(d), making the shell visible. A high-resolution scanning TEM image of the framed region shows the atomic arrangement of the zinc-blende InSb and the epitaxial CdTe.

islands do not merge into a continuous CdTe layer, leaving segments of the InSb nanowire unprotected [Fig. 2(b)]. This discontinuity in the shell manifests as cusps in the CdTe, as shown in transmission electron microscopy (TEM) images acquired along the $\langle 110 \rangle$ zone axis. Within these cusps, the

unprotected InSb locally oxidizes. In contrast, segments of the InSb nanowire covered by CdTe remain oxide free. Importantly, because the CdTe remains crystalline and does not oxidize upon exposure to ambient conditions, it renders the distinction between protected and unprotected InSb segments straightforward. The stability of CdTe against oxidation has been reported [34,35]. The discontinuity in the shell is not visible along the $\langle 112 \rangle$ zone axis, i.e., parallel to a roughly 100-nm-long nanowire facet, because, in projection, crystalline islands are overlaid, causing the discontinuous shell to seem continuous and to appear thicker in TEM. Consequently, TEM measurements overestimate the shell thickness with large errors for short growth times, as demonstrated by the outlying data point for 15 minutes of growth in Fig. 2(a). Using a combination of diffraction and atomic number contrasts, the shell is made visible in annular dark-field (ADF) imaging and is thus measurable since relying only on the atomic number contrast makes the CdTe shell nearly indistinguishable from the InSb [Fig. 2(c)] because the atomic numbers of indium, antimony, cadmium, and tellurium are all very similar (see Sec. S2 of the Supplemental Material for imaging details [24]). To summarize, because of the discontinuity of the shell for short growth times, this growth technique is incompatible with CdTe shells thinner than 2.5 nm.

On the other hand, to achieve continuous CdTe shells thinner than 2.5 nm, a relatively thicker shell can be grown and then etched down to the desired thickness. The shells are etched using atomic hydrogen, instead of using liquid etchants, *in situ* in an MBE chamber to avoid exposing the shells to ambient conditions. The atomic hydrogen flux is created by thermal dissociation of molecular hydrogen in an atomic hydrogen cracker source, where the flux of molecular hydrogen is adjusted using a mass flow controller and the cracking is regulated with the filament temperature. Moreover, atomic hydrogen has been reported to be an effective method for cleaning CdTe surfaces without inducing defects or changing the stoichiometry [36–38]. At a substrate temperature of 400°C, the etched CdTe thickness as a function of time follows a linear relation [Fig. 3(a)] with an etch rate of roughly 0.35 nm/min. Additional etching parameters are provided in the Supplemental Material (Sec. S3) [24]. As disclosed in Figs. 3(c)–3(e), the etching does not induce visible defects in the shell or the InSb nanowire. The smoothness of the etched shells implies that the etching proceeds layer by layer instead of extending isotropically from random spots. Because the etching process is dominated by this layer-by-layer mechanism, the CdTe is completely removed for long etching times, as opposed to being locally removed and leaving behind tiny CdTe islands. When the CdTe shell is completely removed, it leaves the nanowire surfaces exposed, causing the InSb to oxidize upon exposure to ambient air [Fig. 3(e)]. The appearance of this oxide layer demonstrates the effectiveness of the shell in capping the nanowires. The achievable shell thicknesses using this etching method are summarized in Fig. 3(b), where three initial shell thicknesses are considered: 3, 5, and 12.5 nm. For instance, etching the 3-nm CdTe shell for 3 minutes thins down the shell by roughly 1 nm, yielding a 2-nm shell. As indicated by the dashed lines in Fig. 3(b), for all initial shell thicknesses and etching times, a similar linear decrease can be used to describe the etching process.

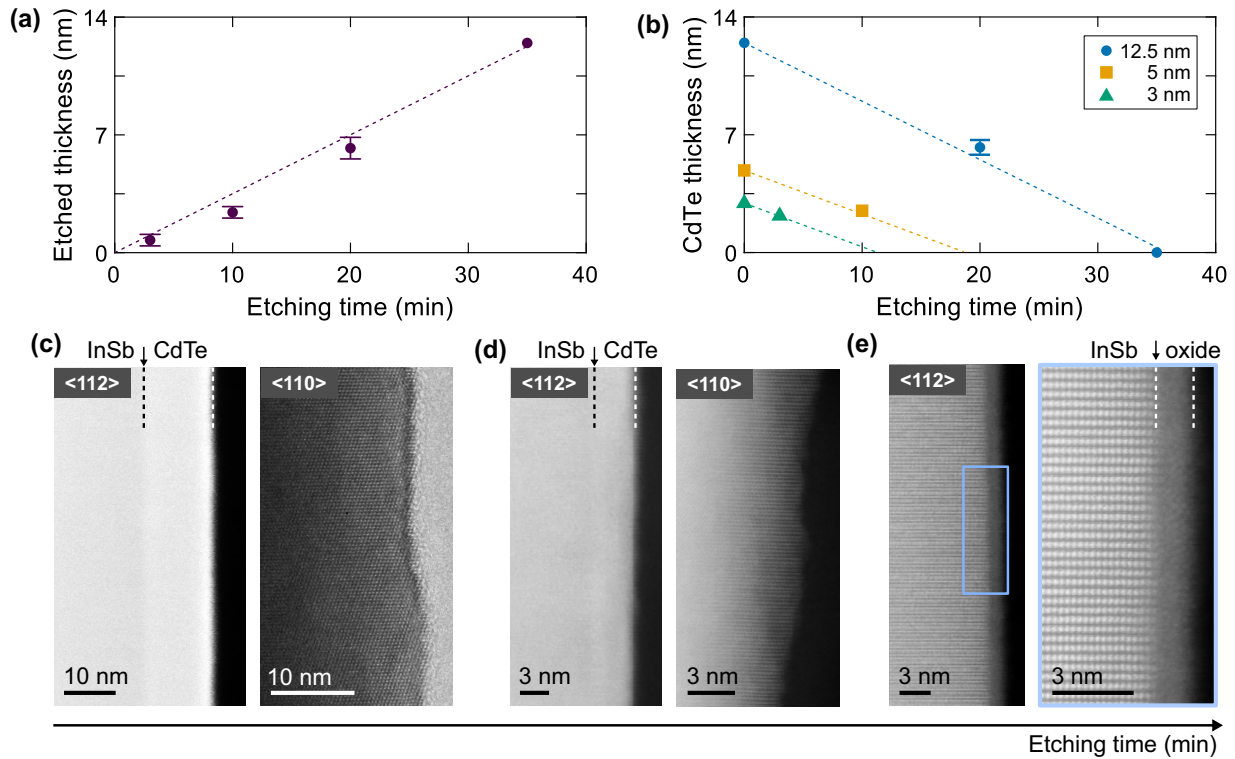


FIG. 3. Etching of CdTe shells for controlled coupling strength. (a) The removed (etched) thickness of CdTe for a given etching time, where a nearly linear dependence dominates the etching process, with an etch rate of roughly 0.35 nm/min. (b) The CdTe shell thicknesses are plotted as a function of etching time, where three starting thicknesses, i.e., 12.5, 5, and 3 nm, are studied. Error bars falling within the size of the data marker are eliminated for clarity. The available data points are used to extrapolate a linear decrease in shell thickness as a function of etching time. (c)–(e) TEM data of 12.5 nm shells etched for 0, 25, and 35 minutes, respectively. (c) The shell is made visible by diffraction contrast imaging, causing the CdTe to appear slightly brighter than the InSb core (ADF-TEM). In the bright-field TEM image, along the $\langle 110 \rangle$ zone axis, the shell does not look atomically flat. (d) Etching for 25 minutes maintains the facet morphology evident along the $\langle 110 \rangle$ zone axis. Atomic hydrogen etching for 25 minutes removes about 8–9 nm of CdTe, resulting in a 3.5 nm shell as determined from the $\langle 112 \rangle$ zone axis ADF-TEM image. (e) Etching for 35 minutes completely removes the CdTe and leaves the InSb nanowire exposed, causing the InSb surface to oxidize.

Because the etching time determines how much of the CdTe is removed, it needs to be adjusted according to both the initial and the final required shell thickness.

Hinging on the obtained results from growth and etching, a combination of both optimally overcomes the limitations imposed by the growth dynamics. Accordingly, uniform CdTe shells with atomic-level control over thickness are made possible. This level of control provides a tuning knob to adjust the coupling strength between the InSb nanowire and the superconductor.

IV. SUPERCONDUCTING SHELLS

To induce superconductivity in the nanowire, it needs to tunnel across the CdTe shell (tunnel barrier). The long coherence length of Al—typically in the micrometer range [39]—makes it particularly compatible with tunneling across a range of differently thick CdTe tunnel barriers (see Fig. 1). Although Al does not rank very highly with regards to superconducting gap, critical temperature, and critical field compared to other single-element type-I superconductors, its small superconducting gap and critical field can be increased by reducing the Al thickness down to a few nanometers [14].

Accordingly, an 8-nm-thick Al shell is deposited on the nanowires in an MBE chamber. The inherent directionality of the molecular beam allows for shadow deposition. In particular, when two structures are placed behind one another, the structure facing the molecular beam shadows the other structure, which enables selective deposition of the superconductor according to the relative alignment of both structures [Figs. 4(a)–4(d)]. In contrast to nonshadowed deposition, the shadowing technique allows for the patterning of the superconductor during its deposition, thus eliminating the need for postfabrication steps such as lithography and etching, which could compromise the properties of hybrid nanowire devices [16,40,41]. Moreover, the vacuum is not broken, promoting cleaner and more pristine interfaces. We selectively deposit Al on nanowires using nanoflakes as shadowing objects, as depicted in the scanning electron microscope (SEM) images of Figs. 4(a)–4(d). The nanoflakes are grown in the same field as the nanowires using the vapor-liquid-solid technique, as detailed in [42]. Depending on their position relative to the nanowire, either a superconducting/normal junction is created or, alternately, a superconducting/normal/superconducting junction is created, as shown in Figs. 4(c) and 4(d).

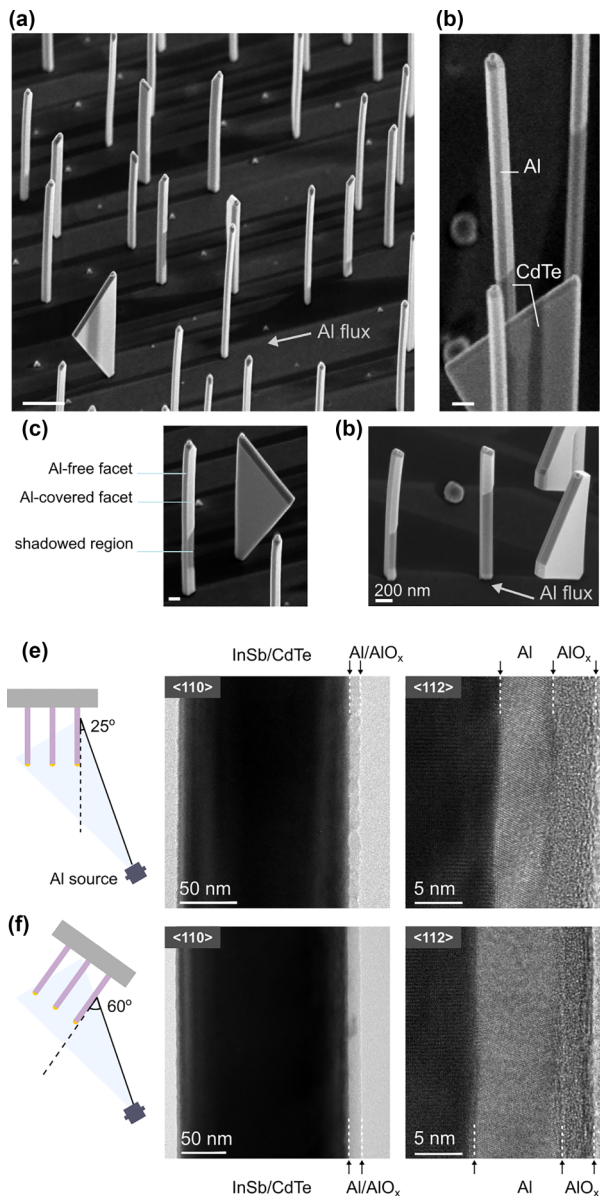


FIG. 4. Shadow deposition of Al. (a) A 30°-tilt view SEM image with directionally deposited Al on a nanowire field (scale bar: 1 μm). (b) Selective deposition of Al via shadowing. The front nanowire casts a shadow on the nanoflake and, simultaneously, the flake shadows the nanowires in the back. The shadowed regions remain Al free (scale bar: 200 nm). (c),(d) The alignment of a nanowire with respect to a nanoflake determines the size and position of a shadow. (c) A small shadow, yielding a superconducting/normal/superconducting junction. Only the facets facing the flux are covered with Al. (d) A large shadow, with only the top part of the nanowire covered with Al, yielding a superconducting/normal junction. (e) The nanowire chip is not tilted with respect to the Al source. The Al flux forms an angle of 25° with the surface of the nanowires. A rough Al shell capped with conformal AlO_x is deposited, visible along the <110> zone axis. Along the <112> zone axis, roughness seems less since in projection it is averaged over the entire facet. Yet, overlapping grains are distinguishable. (f) The nanowire chip is tilted with a 60°-angled deposition of Al, yielding a smooth Al/AlO_x shell. Along the <112> zone axis, individual Al grains are not recognizable. Flat interfaces between the InSb/CdTe core, the Al, and the AlO_x are indicated by arrows.

To promote crystalline growth of Al on the InSb-CdTe nanowires, stringent requirements with regards to the storage conditions of the nanowire chips, the substrate temperature, and the flux angle need to be met. First, to ensure an oxide-free interface between the Al and the CdTe tunnel barrier, the nanowire chips are stored in vacuum after the CdTe shell growth. Second, to suppress possible interface reactions and the high surface diffusion of Al, a low-substrate temperature, in the range of 108–120 K is used, as previously documented for Al on indium arsenide nanowires [15]. Low-substrate temperatures also prevent the Al film from dewetting since Al tends to reduce its surface energy by agglomerating into isolated islands at elevated temperatures. Third, to promote the growth of smooth Al shells, as opposed to grainy rough shells, a large angle between the incoming flux and the surface of the nanowire is employed, as shown in Figs. 4(e) and 4(f). Specifically, because the Al adatoms are rendered highly immobile due to the low-substrate temperatures, the incoming Al molecules end up forming tiny clusters in close proximity to their original landing sites. Therefore, for small flux angles, e.g., 25°, with respect to the nanowire axis, the deposited tiny clusters shadow the region behind them. This self-shadowing leads to a relatively rough Al shell [Fig. 4(e)]. In contrast, a large flux angle of 60° allows the formation of bigger crystalline grains that merge into a smooth Al shell. A similar behavior has been reported for the deposition of niobium on indium arsenide nanowires [43]. The flux angle not only affects the Al shell morphology, but also governs the shell thickness. In particular, for the same deposition rate and duration, the 25°-angle deposition yields a 5 nm shell, as opposed to the 8 nm shell for the 60°-angle deposition [Figs. 4(e) and 4(f)]. Additional details on the Al deposition are provided in Sec. S4 of the Supplemental Material [24]. Importantly, we prevent postdeposition diffusion by oxidizing the Al. The aluminum oxide (AlO_x) layer shown in Figs. 4(e) and 4(f) is created by exposing the nanowire chip to a flow of oxygen, immediately after the Al deposition, which yields a self-terminating AlO_x layer of roughly 3 nm. The AlO_x layer protects the Al shell and prevents the Al from dewetting as it warms up to room temperature.

A representative nanowire covered by a CdTe shell and superconducting Al is provided in Figs. 5(a) and 5(b). The bright-field TEM image taken along the <112> zone axis shows the InSb-CdTe nanowire covered by a polycrystalline Al shell and an amorphous aluminum-oxide (AlO_x). The accompanying elemental dispersive x-ray (EDX) mappings show the composition and the thickness of each layer. While the CdTe shell is 2.5 nm thick, the thickness of the Al and the protective AlO_x are 8 and 3 nm, respectively. As illustrated in Fig. 5(b), the Al shell has an epitaxial relation with the InSb-CdTe core. More generally, all studied Al grains (on several nanowires) exhibit the same crystalline orientation when imaged along the <112> axis of the InSb-CdTe core. In particular, the Al (200) planes are inclined by $24 \pm 2^\circ$ with respect to the InSb (111) planes [Fig. 5(b)]. In contrast, when imaging the same wires along the InSb <110> zone axis, high-resolution TEM images are not able to discern the Al lattice periodicity since in this direction—at the corner between two facets—the projected volume that does not overlap with the core is very small. Thus far, the epitaxial growth of Al on

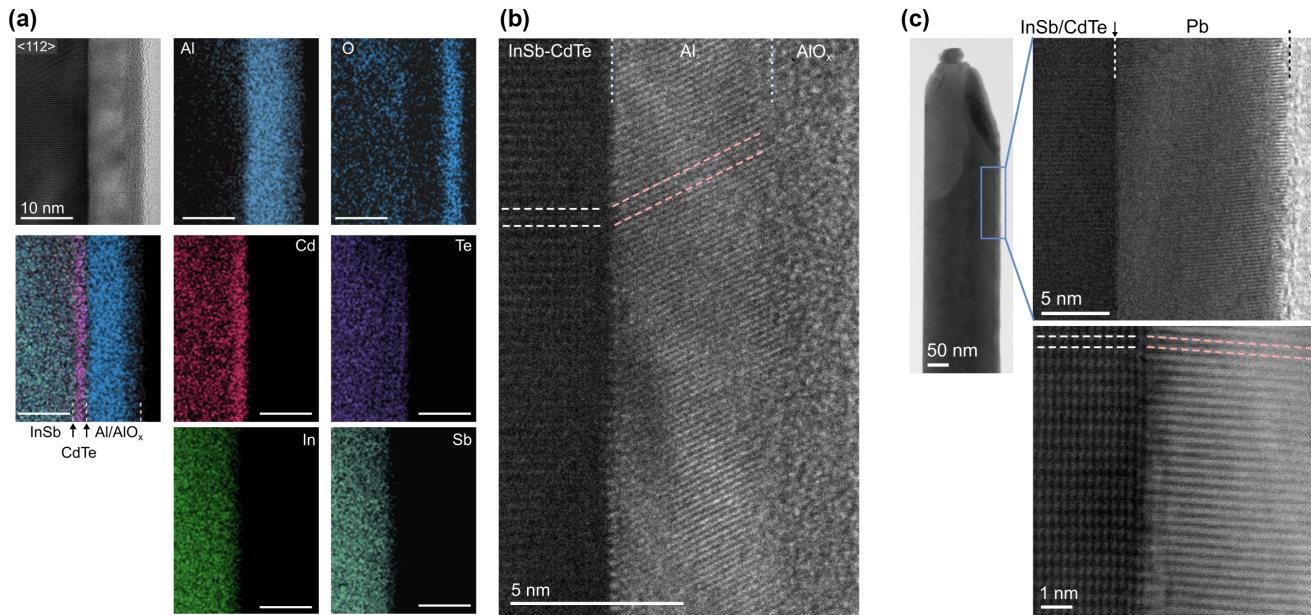


FIG. 5. TEM and EDX analysis of the trilayer composing the nanowire-barrier-superconductor stack. (a) A bright-field TEM image taken along the $\langle 112 \rangle$ zone axis of the stack made up of the InSb nanowire, the CdTe shell, the superconducting Al, and the capping AlO_x . EDX mappings show both individual elements and an overlay, where the InSb, the CdTe, and the Al/ AlO_x layers are identified. Scale bar is 10 nm. (b) A high-resolution bright-field TEM image of the InSb-CdTe-Al interface along the $\langle 112 \rangle$ zone axis. The white dashed lines signify the InSb-CdTe (111) planes, whereas the pink dashed lines indicate the inclined Al (200) planes. (c) A low-magnification bright-field TEM image of a nanowire with a Pb shell. Pb is directionally deposited and is therefore only covering one side. A zoom-in on the framed region reveals a uniform 12-nm Pb shell with a smooth interface. The bright-field STEM image (bottom panel) of the interface shows the inclined attachment of Pb to the surface of the nanowire with defect-free epitaxy. The dashed lines follow the atomic planes of both InSb/CdTe (white) and Pb (pink).

InSb has not been studied in detail. TEM images in a limited number of papers suggest that the epitaxial relation depends on the orientation of the InSb facet [44–46], as expected from the large lattice mismatch. Essentially, with the large difference in lattice constants between Al (4.05 Å) and InSb (6.479 Å), epitaxy is not trivial. Accordingly, little is known about the epitaxial relation between Al and InSb (110) facets. Nevertheless, such an epitaxial relation would likely involve the lateral matching of one of the Al (hkl) planes to the InSb (111) planes at the interface. The epitaxial relation of $1 \times \text{InSb (111)} : 3 \times \text{Al (311)}$ has the smallest residual mismatch of 2.4% compared to other Al (hkl) interplanar distances. Although the Al (311) spacing has not been visualized in our studies, the orientation of the Al (200) planes hints to the $1 \times \text{InSb (111)} : 3 \times \text{Al (311)}$ epitaxy. Specifically, from the cubic crystal structure of Al follows an angle of 25.2° between the Al (311) and the Al (200) planes. This angle is in agreement with the inclination shown in Fig. 5(b). Other epitaxial InSb:Al relations do not yield Al (200) planes with the illustrated inclination. The proposed epitaxial relation implies that upon imaging InSb along the $\langle 112 \rangle$ zone axis, the Al grains are imaged along the $\langle 110 \rangle$ zone axis. Along this viewing axis, both the Al (311) and the Al (200) planes should be visible; however, only the Al (200) are discernible [Fig. 5(b)]. The absence of the Al (311) planes along this viewing direction might be explained by a rotation of the Al grain—due to the residual lattice mismatch—rendering these planes imperceptible along this zone axis.

The interest to perform the same experiments on a superconductor with different properties is motivated by the potential to expand the use of the CdTe shells to other material combinations and determine their corresponding requirements. Lead (Pb), for instance, seems particularly compelling due to its large superconducting gap compared to aluminum. Even though Pb possesses a shorter coherence length, its larger gap, higher critical field, and temperature make it advantageous for experiments with reduced coupling. Specifically, a weaker coupling yields a smaller induced gap. Accordingly, a larger superconducting gap would enable a relatively large induced gap to be resolved in the nanowire even in the case of weak coupling (Fig. 1). Furthermore, the short coherence length of Pb demands different conditions on the CdTe tunnel barriers. Particularly, even thinner CdTe shells are required to allow superconductivity to tunnel into the nanowire while enabling tunability of the superconductor-semiconductor coupling. Initial results of Pb depositions on CdTe-capped InSb nanowires demonstrate that epitaxially aligned Pb shells with smooth interfaces are possible [Fig. 5(c)]. The images in Fig. 5(c) are representative for all five nanowires studied in atomic resolution. The Pb-CdTe interface does not indicate the presence of an interfacial oxide, the existence of which would hinder any epitaxial growth of Pb. All Pb grains have their Pb (111) planes nearly parallel to the InSb (111) planes with a slight misorientation of 2.0° to 5.2° . For the grain displayed in Fig. 5(c), we count 49 InSb (111) planes versus 64 Pb (111) planes. This is a ratio

of 1.306, which nearly yields the $0.374/0.2858 = 1.309$ ratio between the unit-cell parameters of both materials. The small misorientation is likely due to the relaxation of the remaining lattice mismatch [Fig. 5(c)]. Despite the demonstrated smooth and epitaxial Pb-CdTe interface, there remain a few challenges related to the reproducibility of these results and the homogeneity of the deposited Pb across a nanowire chip, likely due to Pb's sensitivity to water [17]. Details of the Pb deposition are given in Sec. S5 of the Supplemental Material [24].

V. CONCLUSIONS

We demonstrate the potential of realizing tunable tunnel barriers using concentric CdTe shells between a semiconducting (InSb) nanowire and a superconductor (Al and Pb). The thicknesses of the shells are predicted to modulate the coupling strength between the semiconductor and the superconductor—that is, the proximity-induced gap. We control the thickness of the shells down to a few monolayers using growth and etching. The CdTe shells also enable the epitaxial growth of the superconductor with a clean, smooth, and abrupt interface, absent of any reactive interface layers or oxides.

These results call for exploring other superconductors with a higher critical field and critical temperature compared to Al. Superconducting tin (Sn) would be of particular interest since it is nearly lattice matched with InSb and CdTe, in addition to its relatively large superconducting gap. The viability of the CdTe shells to serve as tunable tunnel barriers in hybrid nanowire devices can be assessed by studying the proximity-induced gap as a function of the shell thickness in tunneling spectroscopy.

Our InSb nanowires with epitaxial tunnel barriers and epitaxial superconductors potentially provide a new generation of hybrid nanowire devices for probing topological Majorana quasiparticles.

ACKNOWLEDGMENTS

We thank Prof. Jay D. Sau for his guidance on the gap estimate calculations. This work is funded by the Dutch Organization for Scientific Research (NWO), the Foundation for Fundamental Research on Matter (FOM), the European Research Council (ERC HELENA 617256), and Microsoft Corporation Station-Q. Solliance and the Dutch province of Noord-Brabant are acknowledged for funding the TEM facility.

-
- [1] A. Y. Kitaev, Unpaired Majorana fermions in quantum wires, *Phys. Usp.* **44**, 131 (2001).
 - [2] A. Stern and N. H. Lindner, Topological quantum computation—From basic concepts to first experiments, *Science* **339**, 1179 (2013).
 - [3] S. Das Sarma, M. Freedman, and C. Nayak, Majorana zero modes and topological quantum computation, *npj Quantum Inf.* **1**, 15001 (2015).
 - [4] L. Fu and C. L. Kane, Superconducting Proximity Effect and Majorana Fermions at the Surface of a Topological Insulator, *Phys. Rev. Lett.* **100**, 096407 (2008).
 - [5] S. Nadj-Perge, I. K. Drozdov, B. A. Bernevig, and A. Yazdani, Proposal for realizing Majorana fermions in chains of magnetic atoms on a superconductor, *Phys. Rev. B* **88**, 020407(R) (2013).
 - [6] M. Hell, M. Leijnse, and K. Flensberg, Two-Dimensional Platform for Networks of Majorana Bound States, *Phys. Rev. Lett.* **118**, 107701 (2017).
 - [7] R. M. Lutchyn, J. D. Sau, and S. Das Sarma, Majorana Fermions and a Topological Phase Transition in Semiconductor-Superconductor Heterostructures, *Phys. Rev. Lett.* **105**, 077001 (2010).
 - [8] Y. Oreg, G. Refael, and F. von Oppen, Helical Liquids and Majorana Bound States in Quantum Wires, *Phys. Rev. Lett.* **105**, 177002 (2010).
 - [9] A. Y. Kitaev, Fault-tolerant quantum computation by anyons, *Ann. Phys.* **303**, 2 (2003).
 - [10] C. Nayak, S. H. Simon, A. Stern, M. Freedman, and S. Das Sarma, Non-Abelian anyons and topological quantum computation, *Rev. Mod. Phys.* **80**, 1083 (2008).
 - [11] J. Alicea, Majorana fermions in a tunable semiconductor device, *Phys. Rev. B* **81**, 125318 (2010).
 - [12] J. D. Sau, S. Tewari, R. M. Lutchyn, T. D. Stanescu, and S. Das Sarma, Non-Abelian quantum order in spin-orbit-coupled semiconductors: Search for topological Majorana particles in solid-state systems, *Phys. Rev. B* **82**, 214509 (2010).
 - [13] T. D. Stanescu, R. M. Lutchyn, and S. Das Sarma, Majorana fermions in semiconductor nanowires, *Phys. Rev. B* **84**, 144522 (2011).
 - [14] R. M. Lutchyn, E. P. Bakkers, L. P. Kouwenhoven, P. Krogstrup, C. M. Marcus, and Y. Oreg, Majorana zero modes in superconductor–semiconductor heterostructures, *Nat. Rev. Mater.* **3**, 52 (2018).
 - [15] P. Krogstrup, N. Ziino, W. Chang, S. Albrecht, M. Madsen, E. Johnson, J. Nygård, C. M. Marcus, and T. Jespersen, Epitaxy of semiconductor–superconductor nanowires, *Nat. Mater.* **14**, 400 (2015).
 - [16] S. Heedt, M. Quintero-Pérez, F. Borsoi, A. Fursina, N. van Loo, G. P. Mazur, M. P. Nowak, M. Ammerlaan, K. Li, S. Korneychuk *et al.*, Shadow-wall lithography of ballistic superconductor–semiconductor quantum devices, *Nat. Commun.* **12**, 4914 (2021).
 - [17] T. Kanne, M. Marnauza, D. Olsteins, D. J. Carrad, J. E. Sestoft, J. de Bruijckere, L. Zeng, E. Johnson, E. Olsson, K. Grove-Rasmussen *et al.*, Epitaxial Pb on InAs nanowires for quantum devices, *Nat. Nanotechnol.* **16**, 776 (2021).
 - [18] M. Pendharkar, B. Zhang, H. Wu, A. Zarassi, P. Zhang, C. Dempsey, J. Lee, S. Harrington, G. Badawy, S. Gazibegovic *et al.*, Parity-preserving and magnetic field–resilient superconductivity in InSb nanowires with Sn shells, *Science* **372**, 508 (2021).
 - [19] W. Chang, S. Albrecht, T. Jespersen, F. Kuemmeth, P. Krogstrup, J. Nygård, and C. M. Marcus, Hard gap in epitaxial

- semiconductor–superconductor nanowires, *Nat. Nanotechnol.* **10**, 232 (2015).
- [20] S. Takei, B. M. Fregoso, H.-Y. Hui, A. M. Lobos, and S. Das Sarma, Soft Superconducting Gap in Semiconductor Majorana Nanowires, *Phys. Rev. Lett.* **110**, 186803 (2013).
- [21] W. S. Cole, S. Das Sarma, and T. D. Stanescu, Effects of large induced superconducting gap on semiconductor Majorana nanowires, *Phys. Rev. B* **92**, 174511 (2015).
- [22] W. S. Cole, J. D. Sau, and S. Das Sarma, Proximity effect and Majorana bound states in clean semiconductor nanowires coupled to disordered superconductors, *Phys. Rev. B* **94**, 140505(R) (2016).
- [23] C. Reeg, D. Loss, and J. Klinovaja, Metallization of a Rashba wire by a superconducting layer in the strong-proximity regime, *Phys. Rev. B* **97**, 165425 (2018).
- [24] See Supplemental Material at <http://link.aps.org/supplemental/10.1103/PhysRevMaterials.7.016201> for details of the calculation of the proximity-induced gap, transmission electron microscopy imaging, etching parameters, and superconductor deposition.
- [25] G. Badawy, B. Zhang, T. Rauch, J. Momand, S. Koelling, J. Jung, S. Gazibegovic, O. Moutanabbir, B. J. Kooi, S. Botti *et al.*, Electronic structure and epitaxy of CdTe shells on InSb nanowires, *Adv. Sci.* **9**, 2105722 (2022).
- [26] S. Wood, J. Greggi Jr, R. Farrow, W. Takei, F. Shirland, and A. Noreika, Microstructural studies of CdTe and InSb films grown by molecular beam epitaxy, *J. Appl. Phys.* **55**, 4225 (1984).
- [27] E. Luna, A. Trampert, J. Lu, T. Aoki, Y.-H. Zhang, M. R. McCartney, and D. J. Smith, Strategies for analyzing noncommon-atom heterovalent interfaces: The case of CdTe-on-InSb, *Adv. Mater. Interfaces* **7**, 1901658 (2020).
- [28] D. T. F. Marple, Effective electron mass in CdTe, *Phys. Rev.* **129**, 2466 (1963).
- [29] J. D. Sau, R. M. Lutchyn, S. Tewari, and S. Das Sarma, Robustness of Majorana fermions in proximity-induced superconductors, *Phys. Rev. B* **82**, 094522 (2010).
- [30] S. M. Albrecht, A. P. Higginbotham, M. Madsen, F. Kuemmeth, T. S. Jespersen, J. Nygård, P. Krogstrup, and C. Marcus, Exponential protection of zero modes in Majorana islands, *Nature (London)* **531**, 206 (2016).
- [31] M. Deng, S. Vaitiekėnas, E. B. Hansen, J. Danon, M. Leijnse, K. Flensberg, J. Nygård, P. Krogstrup, and C. M. Marcus, Majorana bound state in a coupled quantum-dot hybrid-nanowire system, *Science* **354**, 1557 (2016).
- [32] M. Kjaergaard, M. E. Schwartz, J. Braumüller, P. Krantz, J. I.-J. Wang, S. Gustavsson, and W. D. Oliver, Superconducting qubits: Current state of play, *Annu. Rev. Condens. Matter Phys.* **11**, 369 (2020).
- [33] G. Badawy, S. Gazibegovic, F. Borsoi, S. Heedt, C.-A. Wang, S. Koelling, M. A. Verheijen, L. P. Kouwenhoven, and E. P. Bakkers, High mobility stemless InSb nanowires, *Nano Lett.* **19**, 3575 (2019).
- [34] A. Ebina and T. Takahashi, Studies of clean and adatom treated surfaces of II–VI compounds, *J. Cryst. Growth* **59**, 51 (1982).
- [35] B. Kowalski, B. Orłowski, and J. Ghijsen, XPS study of CdTe (110) surface oxidation process, *Surf. Sci.* **412-413**, 544 (1998).
- [36] Y. Luo, D. Slater, M. Levy, and R. Osgood Jr, Chemical preparation of CdTe (100) and (110) surfaces using atomic hydrogen, *Appl. Surf. Sci.* **104-105**, 49 (1996).
- [37] Y. Luo, D. Slater, and R. Osgood Jr, Low-damage processing of CdTe (110) surfaces using atomic hydrogen, *Appl. Phys. Lett.* **67**, 55 (1995).
- [38] L. Hirsch, Z. Yu, S. Buczkowski, T. Myers, and M. Richards-Babb, The use of atomic hydrogen for substrate cleaning for subsequent growth of II-VI semiconductors, *J. Electron. Mater.* **26**, 534 (1997).
- [39] T. Kiendl, F. von Oppen, and P. W. Brouwer, Proximity-induced gap in nanowires with a thin superconducting shell, *Phys. Rev. B* **100**, 035426 (2019).
- [40] D. J. Carrad, M. Bjergfelt, T. Kanne, M. Aagesen, F. Krizek, E. M. Fiordaliso, E. Johnson, J. Nygård, and T. S. Jespersen, Shadow epitaxy for *in situ* growth of generic semiconductor/superconductor hybrids, *Adv. Mater.* **32**, 1908411 (2020).
- [41] S. A. Khan, C. Lampadaris, A. Cui, L. Stampfer, Y. Liu, S. J. Pauka, M. E. Cachaza, E. M. Fiordaliso, J.-H. Kang, S. Korneychuk *et al.*, Highly transparent gatable superconducting shadow junctions, *ACS Nano* **14**, 14605 (2020).
- [42] S. Gazibegovic, G. Badawy, T. L. Buckers, P. Leubner, J. Shen, F. K. de Vries, S. Koelling, L. P. Kouwenhoven, M. A. Verheijen, and E. P. Bakkers, Bottom-up grown 2d InSb nanostructures, *Adv. Mater.* **31**, 1808181 (2019).
- [43] N. A. Güsken, T. Rieger, P. Zellekens, B. Bennemann, E. Neumann, M. I. Lepsa, T. Schäpers, and D. Grützmacher, MBE growth of Al/InAs and Nb/InAs superconducting hybrid nanowire structures, *Nanoscale* **9**, 16735 (2017).
- [44] R. L. Op het Veld, D. Xu, V. Schaller, M. A. Verheijen, S. M. Peters, J. Jung, C. Tong, Q. Wang, M. W. de Moor, B. Hesselmann *et al.*, In-plane selective area InSb–Al nanowire quantum networks, *Commun. Phys.* **3**, 59 (2020).
- [45] C. Thomas, R. E. Diaz, J. H. Dycus, M. E. Salmon, R. E. Daniel, T. Wang, G. C. Gardner, and M. J. Manfra, Toward durable Al-InSb hybrid heterostructures via epitaxy of 2 ml interfacial InAs screening layers, *Phys. Rev. Mater.* **3**, 124202 (2019).
- [46] S. T. Gill, J. Damasco, B. E. Janicek, M. S. Durkin, V. Humbert, S. Gazibegovic, D. Car, E. P. Bakkers, P. Y. Huang, and N. Mason, Selective-area superconductor epitaxy to ballistic semiconductor nanowires, *Nano Lett.* **18**, 6121 (2018).